

Experimental Study of $\rho \rightarrow \pi^0\pi^0\gamma$ and $\omega \rightarrow \pi^0\pi^0\gamma$ Decays

M.N.Achasov, K.I.Beloborodov, A.V.Berdyugin, A.G.Bogdanchikov,
A.V.Bozhenok, D.A.Bukin, S.V.Burdin, A.V.Vasiljev, V.B.Golubev,
T.V.Dimova, V.P.Druzhinin*, V.N.Ivanchenko, A.A.Korol, I.A.Koop,
S.V.Koshuba, A.V.Otboev, E.V.Pakhtusova, A.A.Salnikov,
S.I.Serednyakov, V.A.Sidorov, Z.K.Silagadze, A.N.Skrinsky,
A.G.Skripkin, Yu.V.Usov, V.V.Shary, Yu.M.Shatunov.

Budker Institute of Nuclear Physics,
Novosibirsk State University,
Novosibirsk 630090, Russia

Abstract

The $e^+e^- \rightarrow \pi^0\pi^0\gamma$ process was studied in the SND experiment at VEPP-2M e^+e^- collider in the energy region 0.60–0.97 GeV. From the analysis of the energy dependence of measured cross section the branching ratios $B(\omega \rightarrow \pi^0\pi^0\gamma) = (6.6_{-0.8}^{+1.4} \pm 0.6) \cdot 10^{-5}$ and $B(\rho \rightarrow \pi^0\pi^0\gamma) = (4.1_{-0.9}^{+1.0} \pm 0.3) \cdot 10^{-5}$ were obtained.

PACS: 13.65.+i, 14.40.Cs

1 Introduction

In 1998 and 2000 the experiments with Spherical Neutral Detector (SND)[1] at VEPP-2M e^+e^- collider were carried out in the energy range $E = 360 - 970$ MeV where cross section of e^+e^- annihilation into hadrons is determined by the ρ and ω meson decays. The integrated luminosity of 9 pb^{-1} collected in the experiment corresponds to $3.5 \cdot 10^6$ and $7 \cdot 10^6$ produced ρ and ω mesons, respectively. One of the goals of the experiment was the investigation of the rare process

$$e^+e^- \rightarrow \rho, \omega \rightarrow \pi^0\pi^0\gamma. \quad (1)$$

*e-mail: druzhinin@inp.nsk.su

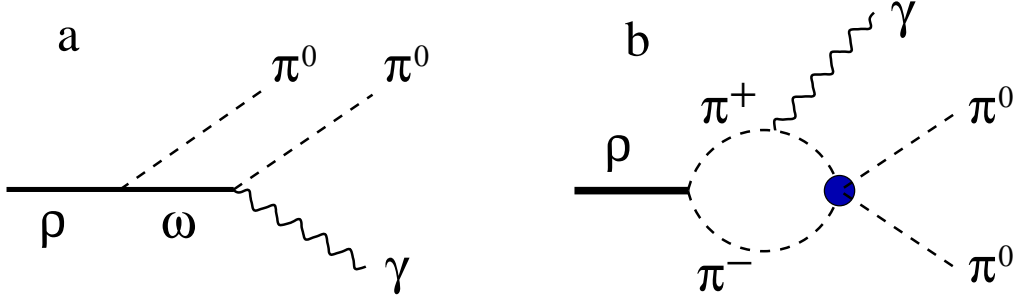


Figure 1: Two mechanism of $\rho \rightarrow \pi^0 \pi^0 \gamma$ decay: (a) is the VMD mechanism, (b) is the transition through pion loop.

Our preliminary study [2] of the process (1) was based on 1/3 of collected statistics. Its results were the first measurement of $B(\rho \rightarrow \pi^0 \pi^0 \gamma) = (4.8_{-1.8}^{+3.4} \pm 0.2) \cdot 10^{-5}$ and the measurement of $B(\omega \rightarrow \pi^0 \pi^0 \gamma) = (7.8 \pm 2.7 \pm 2.0) \cdot 10^{-5}$ confirming the only previous measurement of this decay by GAMS: $B(\omega \rightarrow \pi^0 \pi^0 \gamma) = (7.2 \pm 2.5) \cdot 10^{-5}$ [3].

The theoretical study of the $\rho, \omega \rightarrow \pi^0 \pi^0 \gamma$ decays was begun by P.Singer in Ref. [4] where the transitions via $\omega \pi^0$ (Fig. 1a) and $\rho^0 \pi^0$ intermediate states were suggested. The vector meson dominance (VMD) calculation with these intermediate states leads to branching ratios $\sim 1 \cdot 10^{-5}$ and $\sim 3 \cdot 10^{-5}$ for $\rho \rightarrow \pi^0 \pi^0 \gamma$ and $\omega \rightarrow \pi^0 \pi^0 \gamma$, respectively [5].

For $\rho \rightarrow \pi^0 \pi^0 \gamma$ decay another mechanism through the pions loops (Fig. 1b) is also possible [5]. The branching ratios expected for this mechanism in different models [6, 7, 8, 9] are listed in Table 1. It was noted in Ref. [8] that the $\rho \rightarrow \pi^0 \pi^0 \gamma$ decay via chiral loops can be interpreted as $\rho \rightarrow \sigma \gamma$, where σ is a scalar state decaying into $\pi\pi$ pair. The dependence of $B(\rho \rightarrow \pi^0 \pi^0 \gamma)$ on σ parameters was studied in Ref. [7]. The range of $B(\rho \rightarrow \pi^0 \pi^0 \gamma)$ values in $L\sigma M$ model corresponds to different σ widths. Since the amplitudes of

Table 1: The branching ratios for different contributions to $\rho \rightarrow \pi^0 \pi^0 \gamma$ decay. The chiral loop or $\rho \rightarrow \sigma \gamma$ contribution is calculated in the framework of Chiral Perturbation Theory (χPT) [6, 7], Unitarized Chiral Perturbation Theory ($U\chi PT$) [8, 9], Linear Sigma Model ($L\sigma M$) [7] and σ pole model [10].

model	VMD	loops, $\sigma \gamma$	total
χPT	$1.3 \cdot 10^{-5}$	$1.0 \cdot 10^{-5}$	$2.9 \cdot 10^{-5}$
$U\chi PT$	$1.5 \cdot 10^{-5}$	$1.5 \cdot 10^{-5}$	$4.2 \cdot 10^{-5}$
$L\sigma M$	$1.3 \cdot 10^{-5}$	$(0.8 - 2.1) \cdot 10^{-5}$	$(2.8 - 4.7) \cdot 10^{-5}$
σ pole	$1.0 \cdot 10^{-5}$	$\sim 2 \cdot 10^{-3}$	$\sim 2 \cdot 10^{-3}$

$\rho \rightarrow \omega \pi^0 \rightarrow \pi^0 \pi^0 \gamma$ transition (Fig. 1a) and of the pion loops (Fig. 1b) are of the same order of magnitude, their interference is substantial. The interference contribution into branching ratio is predicted to be positive. The theoretical values for the total branching ratios are also listed in Table 1. The predictions of the chiral models [6, 7, 8, 9] are in agreement with our previous experimental result. The significantly larger value of $B(\rho \rightarrow \pi^0 \pi^0 \gamma)$ was obtained in Ref. [10] using σ pole model. Their result contradicts to existing experimental data.

In $\omega \rightarrow \pi^0 \pi^0 \gamma$ decay the contribution of pion loops is G -parity suppressed while the contribution of kaon loop is small due to large kaon mass. Therefore, it is assumed that the $\omega \rightarrow \pi^0 \pi^0 \gamma$ decay proceeds through $\rho^0 \pi^0$ intermediate state. The first measurement $B(\omega \rightarrow \pi^0 \pi^0 \gamma) = (7.2 \pm 2.5) \cdot 10^{-5}$ [3] significantly exceeded the existent prediction of VMD model: $3 \cdot 10^{-5}$ [5]. An attempt to explain this discrepancy was done in Ref. [11] where ρ - ω mixing was taken into account and coupling constants were extracted from experimental values of $\Gamma(\omega \rightarrow 3\pi)$ and $\Gamma(\rho^0 \rightarrow \pi^0 \gamma)$. As a result the estimated value of $B(\omega \rightarrow \pi^0 \pi^0 \gamma)$ increased up to $(4.6 \pm 1.1) \cdot 10^{-5}$. Similar results $(4.5-4.7) \cdot 10^{-5}$ were then obtained in Refs. [6, 9]. In Ref. [12] the large experimental value of $B(\omega \rightarrow \pi^0 \pi^0 \gamma)$ was explained by additional contribution of the $\omega \rightarrow \sigma \gamma$ transition and used to extract the value of $g_{\omega \sigma \gamma}$ coupling constant.

In the present work we present the experimental results on $B(\omega \rightarrow \pi^0 \pi^0 \gamma)$ and $B(\rho \rightarrow \pi^0 \pi^0 \gamma)$ based on full SND data sample.

2 Event selection

For analysis five-photon events with the energy deposition in the calorimeter

$$E_{tot} > 0.7 \cdot E \quad (2)$$

and the total momentum measured by the calorimeter

$$P_{tot} < 0.15 \cdot E/c \quad (3)$$

were selected. Here E is e^+e^- center of mass energy.

Due to high beam background rate in 5% of events fake photons appear. This makes possible for lower photon multiplicity QED processes $e^+e^- \rightarrow 2\gamma, 3\gamma, 4\gamma$, and $\rho, \omega \rightarrow \pi^0 \gamma, \eta \gamma \rightarrow 3\gamma$ decays to imitate five-photon events producing main background contribution for the process under study. Detector response to the beam background was studied using special events recorded with a random generator trigger. The information on the fired detector channels in these events was used for simulation of the process under

study and the background processes. Considerable suppression (by a factor of 8) of the background from events with fake photons was achieved by imposing the following cuts:

$$E_{min} > 30 \text{ MeV}, 30^\circ < \theta_{min} < 150^\circ, \quad (4)$$

where E_{min} and θ_{min} are the energy and polar angle of the softest photon in an event. These cuts reduce the detection efficiency for the process under study by 25%. Another background source is the $e^+e^- \rightarrow \eta\gamma \rightarrow 3\pi^0\gamma \rightarrow 7\gamma$ reaction producing five-photon events mainly due to the merging of near photons. To suppress this background, the parameter χ_γ describing transverse energy deposition profile of the detected photon [13] was used. The cut

$$\chi_\gamma < 5 \quad (5)$$

suppresses the $e^+e^- \rightarrow \eta\gamma$ background by a factor of 2 with a 5% loss of actual 5-photon events.

Further selection was based on the kinematic fitting of the events. Compatibility of the event kinematics with $e^+e^- \rightarrow 5\gamma$ and $e^+e^- \rightarrow 3\gamma$ hypotheses was checked. For the 3γ hypothesis two out of five photons were considered spurious: all 3γ subsets were tested and the best one with minimum χ^2 value was selected. As a result of kinematic fitting the χ^2 values, $\chi_{5\gamma}$ and $\chi_{3\gamma}$, were calculated for both hypotheses. The cut

$$\chi_{3\gamma} > 20 \quad (6)$$

practically eliminates $e^+e^- \rightarrow 2\gamma, 3\gamma$ background with the loss only 2.5% of the events of the process under study. Figure 2 depicts the $\chi_{5\gamma}$ distribution of the experimental and simulated events. The following cut was imposed on this parameter:

$$\chi_{5\gamma} < 20. \quad (7)$$

Finally, the events with two π^0 mesons were selected. To do this the kinematic fit in $e^+e^- \rightarrow \pi^0\pi^0\gamma$ hypothesis was performed and the following cut was imposed:

$$\chi_{\pi\pi\gamma} - \chi_{5\gamma} < 10. \quad (8)$$

Here $\chi_{\pi\pi\gamma}$ is the χ^2 value of the kinematic fit for the $e^+e^- \rightarrow \pi^0\pi^0\gamma$ hypothesis. The $\chi_{\pi\pi\gamma} - \chi_{5\gamma}$ distributions for the experimental and simulated events are shown in Fig.3.

The difference between distributions of the background events and events of the process under study (Figs. 2 and 3) was used to estimate the accuracy of the background calculation. The experimental distribution was fitted by

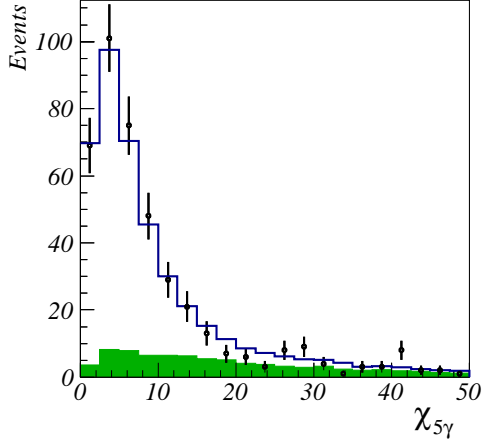


Figure 2: The $\chi_{5\gamma}$ distribution. Points with error bars represent experimental data. The histogram is a simulation of the process (1) and background processes. The shaded histogram shows the contribution of background processes.

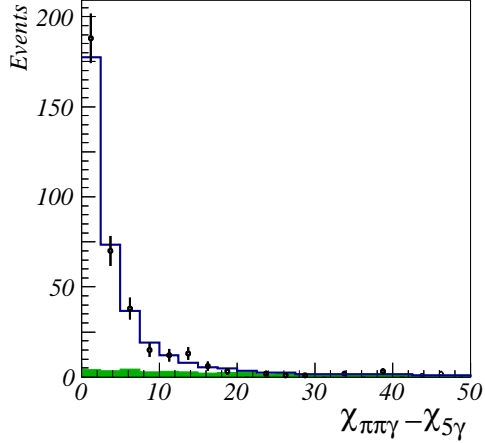


Figure 3: The $\chi_{\pi\pi\gamma} - \chi_{5\gamma}$ distribution. The points with error bars are experimental data. The histogram is the sum of simulated events of the process (1) and background processes. The shaded histogram is the contribution of the background processes.

the sum of simulated distributions for the process (1) and background. As a result of the fit the ratio $K = N_{exp}^{bkg} / N_{calc}^{bkg} = 0.7 \pm 0.2$ was determined. For softer selection criteria without cuts (4,6,5) this ratio is equal to 1.30 ± 0.05 and does not depend on the beam energy at our level of statistical accuracy. From this we conclude that the systematic error of the background estimation does not exceed 50%.

The total of 310 events were selected with estimated background of 15 ± 7 events. The main sources of the residual background are $e^+e^- \rightarrow \eta\gamma$ and $e^+e^- \rightarrow 4\gamma$ processes. The distribution of selected events and calculated background over center of mass energy is given in the Table 2. No events were detected below 600 MeV. The uncertainty of the center of mass energy, integrated luminosity, and detection efficiency are listed in Table 2 for each energy point. The uncertainty of the center of mass energy includes the beam energy spread and the energy shift between 1998 and 2000 scans. The integrated luminosity was measured using $e^+e^- \rightarrow \gamma\gamma$ process. The statistical error of the luminosity in each energy point does not exceed 1% and is not included in the table. Its systematic error was estimated to be 3%. The detection efficiency for the process (1) was determined by simulation. The differential cross section of the $e^+e^- \rightarrow \pi^0\pi^0\gamma$ process calculated in VMD model [14] was used for simulation. The systematic error of the detection

efficiency, including the model error due to possible contribution from $\sigma\gamma$ intermediate state was estimated to be 5%.

3 Fitting of the cross section

The fitting procedure maximizes the logarithmic likelihood function

$$L = \sum_i \ln P_i(N_i^{exp}, N_i^{th}),$$

where P_i is a Poisson probability to detect observed number of events N_i^{exp} in the i -th energy bin with a theoretical expectation of N_i^{th} . The theoretical expectations were calculated as

$$N_i^{th} = \varepsilon_i L_i \sigma(E_i) (1 + \delta(E_i)) + N_i^{bkg},$$

where N_i^{bkg} is a calculated number of background events, ε_i is a detection efficiency, L_i is the integrated luminosity, $\sigma(E)$ is $e^+e^- \rightarrow \pi^0\pi^0\gamma$ cross section depending on a set of approximation parameters, δ is a radiative correction. The radiative correction, which is a functional of the cross-section energy dependence $\sigma(E)$ [15], was determined within the fitting procedure. The values of radiative correction evaluated for each experimental energy point are listed in Table 2. The model error of the $(1 + \delta)$ value does not exceed 3%. The values of the experimental cross section calculated as

$$\sigma_i^{exp} = \frac{N_i^{exp} - N_i^{bkg}}{\varepsilon_i L_i (1 + \delta(E_i))}$$

are shown in Fig.4 and listed in Table 2. The systematic error of the cross section is determined by the errors of the detector efficiency, integrated luminosity, and radiative correction. It was estimated to be 7%.

To calculate the cross section $\sigma(E)$ the amplitude of the $e^+e^- \rightarrow \pi^0\pi^0\gamma$ process was parametrized as

$$A_{\pi\pi\gamma} = A_{\rho\omega\pi}(BW_\rho + \alpha_1 BW_{\rho'} + \alpha_2 BW_{\rho''}) + \beta A_{\rho\sigma\gamma} BW_\rho + \gamma A_\omega BW_\omega, \quad (9)$$

The first term in Eq.(9) is the amplitude of the $e^+e^- \rightarrow \rho, \rho', \rho'' \rightarrow \omega\pi^0$, where ρ' and ρ'' are excitations of the $\rho(770)$. Second and third terms are $e^+e^- \rightarrow \rho(770) \rightarrow \sigma\gamma \rightarrow \pi^0\pi^0\gamma$ and $e^+e^- \rightarrow \omega \rightarrow \pi^0\pi^0\gamma$ amplitudes. Each amplitude is written in a factorized form. The functions $A_{\rho\omega\pi^0}$, $A_{\rho\sigma\gamma}$, A_ω depending on the momenta of final particles describe the dynamics of vector

Table 2: Center of mass energy E , its standard deviation σ_E , integrated luminosity L , number of selected events N_{exp} , calculated number of background events N_{bkg} , detection efficiency ε , radiative correction $1 + \delta$ and the $e^+e^- \rightarrow \pi^0\pi^0\gamma$ cross section σ^{exp} .

E, MeV	σ_E, MeV	L, nb^{-1}	N_{exp}	N_{bkg}	ε	$1 + \delta$	σ^{exp}, nb
600.1	0.29	88.3	0	0.1	0.273	0.912	$-0.005^{+0.052}_{-0.002}$
630.1	0.30	116.1	0	0.1	0.269	0.906	$-0.004^{+0.041}_{-0.002}$
660.2	0.25	271.6	2	0.3	0.273	0.900	$0.025^{+0.040}_{-0.019}$
690.2	0.29	167.2	2	0.2	0.263	0.895	$0.046^{+0.067}_{-0.033}$
720.3	0.26	588.5	1	0.8	0.251	0.892	$0.002^{+0.018}_{-0.007}$
750.2	0.32	219.0	3	0.1	0.259	0.897	$0.057^{+0.057}_{-0.032}$
760.2	0.31	238.9	2	0.3	0.251	0.896	$0.032^{+0.049}_{-0.024}$
764.2	0.32	250.4	5	0.2	0.254	0.892	$0.085^{+0.060}_{-0.038}$
770.2	0.31	284.4	8	0.3	0.253	0.877	$0.122^{+0.063}_{-0.044}$
774.2	0.34	217.1	7	0.2	0.252	0.855	$0.145^{+0.081}_{-0.055}$
778.1	0.34	247.9	6	0.5	0.261	0.820	$0.104^{+0.068}_{-0.045}$
780.2	0.35	319.5	16	1.2	0.263	0.807	$0.218^{+0.075}_{-0.059}$
781.1	0.33	339.6	20	1.2	0.267	0.807	$0.257^{+0.076}_{-0.061}$
782.1	0.31	656.3	34	1.0	0.257	0.815	$0.240^{+0.050}_{-0.042}$
783.2	0.30	473.4	30	2.0	0.253	0.833	$0.280^{+0.066}_{-0.055}$
784.2	0.32	346.2	24	0.7	0.261	0.857	$0.301^{+0.077}_{-0.063}$
785.3	0.24	212.3	12	0.4	0.257	0.890	$0.238^{+0.094}_{-0.070}$
786.1	0.33	267.7	11	0.4	0.255	0.914	$0.170^{+0.071}_{-0.052}$
790.1	0.34	191.4	4	0.3	0.258	1.006	$0.074^{+0.064}_{-0.039}$
794.2	0.34	206.7	1	0.2	0.256	1.044	$0.014^{+0.042}_{-0.015}$
800.2	0.32	276.8	10	0.3	0.255	1.053	$0.130^{+0.057}_{-0.042}$
810.2	0.34	279.5	3	0.4	0.240	1.043	$0.037^{+0.030}_{-0.024}$
820.1	0.36	315.2	2	0.3	0.244	1.035	$0.021^{+0.033}_{-0.016}$
840.2	0.35	677.5	8	0.8	0.247	1.025	$0.042^{+0.023}_{-0.016}$
880.0	0.41	376.0	7	0.5	0.222	1.001	$0.078^{+0.045}_{-0.031}$
919.9	0.44	478.6	8	0.3	0.256	0.916	$0.069^{+0.035}_{-0.025}$
939.9	0.43	469.0	22	0.7	0.248	0.856	$0.214^{+0.058}_{-0.047}$
949.7	0.32	261.7	20	0.3	0.261	0.855	$0.338^{+0.095}_{-0.076}$
957.7	0.32	233.9	13	0.2	0.263	0.858	$0.242^{+0.089}_{-0.067}$
969.7	0.34	251.5	29	0.5	0.250	0.865	$0.524^{+0.119}_{-0.099}$

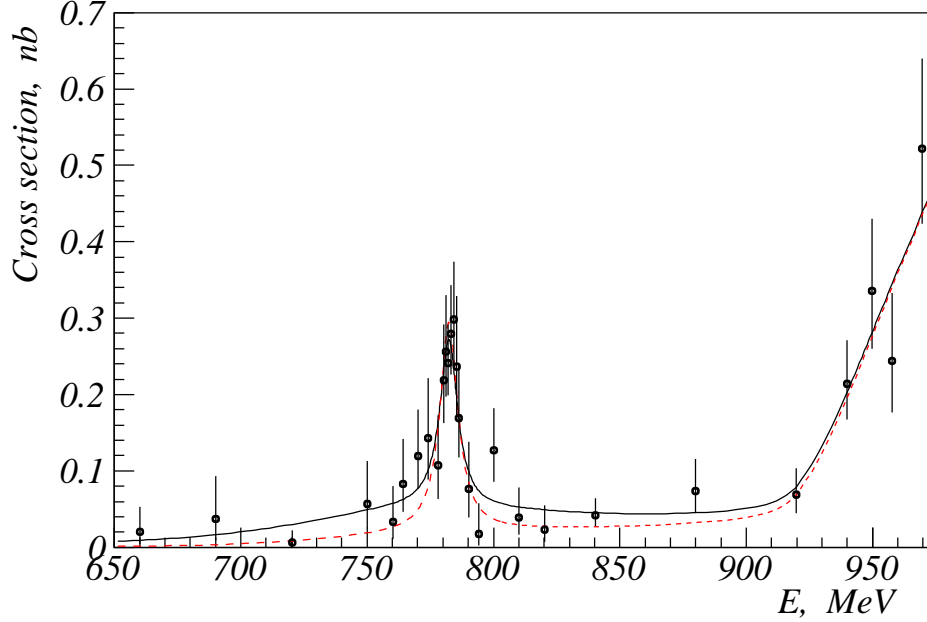


Figure 4: The cross section of the $e^+e^- \rightarrow \pi^0\pi^0\gamma$ process. Points with error bars are experimental data. Solid line is a result of fitting in the model 3 of Table 5. The dashed line corresponds to the fit with $B(\rho \rightarrow \sigma\gamma) = 0$.

mesons decays. The functions BW_i describe the Breit-Wigner resonance shapes:

$$BW_i = \frac{m_i^2}{m_i^2 - E^2 - iE\Gamma_i(E)}, \quad i = \rho, \rho', \rho'', \omega.$$

Here m_i and $\Gamma_i(E)$ are resonance mass and energy dependent width. The cross section is calculated from Eq.(9) by integration over the phase space of final particles: $\sigma(E) = \int |A_{\pi\pi\gamma}|^2 d\Pi$. At the energy above $\omega\pi$ threshold the Breit-Wigner functions of ρ mesons are modified $BW_{\rho_i} \rightarrow BW_{\rho_i} C_{\rho_i\omega\pi}$, where $C_{\rho_i\omega\pi}$ are Blatt-Weisskopf factors, restricting fast growth of the $\Gamma_{\rho_i\omega\pi}$ partial widths [16]:

$$C_{\rho\omega\pi} = \frac{1}{\sqrt{1 + (Rq_\omega(E))^2}}, \quad C_{\rho_i\omega\pi} = \sqrt{\frac{1 + (Rq_\omega(m_{\rho_i}))^2}{1 + (Rq_\omega(E))^2}}, \quad \rho_i = \rho', \rho''. \quad (10)$$

Here q_ω is the ω meson momentum in $\rho_i \rightarrow \omega\pi$ decay. The range parameter R is supposed to be the same for ρ, ρ', ρ'' mesons. The main decay modes of ρ mesons were taken into account for calculation of the energy dependence of the resonance widths. For instance, in the case of $\rho(770)$ we use the following

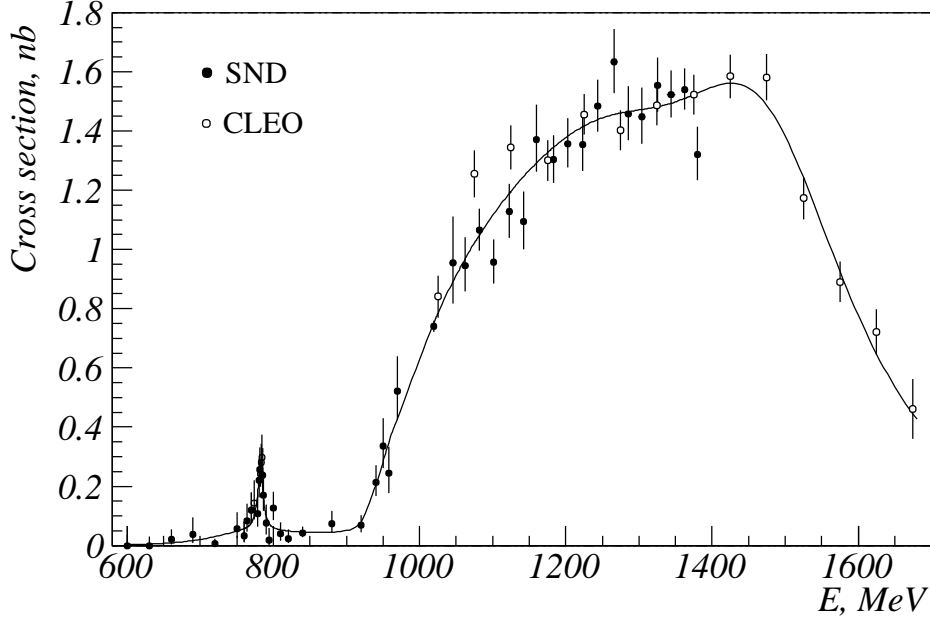


Figure 5: The cross section of the $e^+e^- \rightarrow \pi^0\pi^0\gamma$ reaction. Points with error bars are experimental data. Curve is a fit result in the model 3 of Table 5.

expression:

$$\Gamma_\rho(E) = \Gamma_\rho(m_\rho) \left(\frac{m_\rho}{E} \right)^2 \left(\frac{q_\pi(E)}{q_\pi(m_\rho)} \right)^3 C_{\rho\pi\pi}^2 + \frac{g_{\rho\omega\pi}^2}{12\pi} q_\omega^3(E) C_{\rho\omega\pi}^2. \quad (11)$$

Here q_π is a pion momentum in the $\rho \rightarrow 2\pi$ decay. The Blatt-Weisskopf factor $C_{\rho\pi\pi}$ is expressed by the formula similar to Eq.(10).

The amplitude of the $e^+e^- \rightarrow \omega\pi$ process is described by formulas from Ref. [14, 17] and depends on 8 parameters. The data from energy region below 1 GeV are insufficient to determine them. Therefore we used additional measurements of the $e^+e^- \rightarrow \omega\pi^0$ cross section in the 1–1.4 GeV energy range by SND [17] and of the $\omega\pi^0$ spectral function in $\tau \rightarrow \omega\pi\nu_\tau$ decay by CLEO [18]. The spectral function can be converted to corresponding production cross section in e^+e^- collisions using CVC hypothesis [19]. The all-data fit on $e^+e^- \rightarrow \pi^0\pi^0\gamma$ cross section is shown in Fig.5. For $E > 1$ GeV experimental data are well described by three models with parameters listed in Table 3. The ranges of parameter values correspond to the variation of the parameter R from 0 to 2 GeV^{-1} . The statistical errors are not shown because they are significantly smaller than model biases. For models with two excited ρ states the ρ' mass and width were fixed to 1400 MeV and 500 MeV. These values are close to ρ' parameters from $\pi^\pm\pi^0$ spectral function data [20, 21].

Table 3: Parameters of the models describing $e^+e^- \rightarrow \omega\pi \rightarrow \pi^0\pi^0\gamma$ cross section for $E > 1$ GeV.

	$g_{\rho\omega\pi}$	$m_{\rho'}$	$\Gamma_{\rho'}$	α_1	$m_{\rho''}$	$\Gamma_{\rho''}$	α_2
1	14.3-15.8	—	—	—	1630-1710	630-1000	-(0.19-0.24)
2	14.1-15.7	1400	500	-(0.04-0.06)	1580-1620	420-580	-(0.14-0.18)
3	15.4-16.6	1400	500	-(0.39-0.42)	1560-1640	380-780	0.24-0.30

Below $\omega\pi^0$ threshold the amplitude of the $e^+e^- \rightarrow \omega\pi^0$ process drops rapidly and the product $|BW_\rho|^2 \int |A_{\rho\omega\pi}|^2 d\Pi$ in contrast with the corresponding product for $\rho \rightarrow \sigma\gamma$ transition does not demonstrate resonance behavior. This allows to separate contributions of the two ρ decay mechanisms by measurement of energy dependence of the $e^+e^- \rightarrow \pi^0\pi^0\gamma$ cross section. The $\rho \rightarrow \sigma\gamma$ decay amplitude was described by the χPT and $L\sigma M$ models from Ref. [7]. The three sets of σ parameters [22, 23, 7] used in the $L\sigma M$ model are listed in Table 5. The χPT model corresponds to $m_\sigma \rightarrow \infty$. The β parameter represents the difference between observed value of the $\rho \rightarrow \sigma\gamma$ decay amplitude and theoretical prediction.

For $\omega \rightarrow \pi^0\pi^0\gamma$ decay the variation of the final state phase in the CMS energy interval of the ω meson is small, so we cannot separate different decay mechanisms studying the cross section energy dependence. Thus the amplitude of the $\omega \rightarrow \pi^0\pi^0\gamma$ decay was written according to VMD model [14]. The ρ - ω mixing was taken into account following Ref. [7]. Possible contributions of other mechanisms would result in a deviation of the complex parameter γ from 1.

Full description of the energy dependence of the cross section below 1 GeV requires extra four parameters e.g. absolute values and phases of β and γ : $|\beta|$, ϕ_β , $|\gamma|$, ϕ_γ . But we prefer two other sets of parameters: $B(\rho \rightarrow \sigma\gamma)$, ϕ_β , $B(\omega \rightarrow \pi^0\pi^0\gamma)$, ϕ_γ or $B(\rho \rightarrow \pi^0\pi^0\gamma)$, ϕ_β , $B(\omega \rightarrow \pi^0\pi^0\gamma)$, ϕ_γ . The branching ratios are related to β and γ as

$$B(\rho \rightarrow \pi^0\pi^0\gamma) = \frac{m_\rho^2}{\Gamma_\rho^2} \frac{1}{\sigma_\rho} \int |A_{\rho\omega\pi}(m_\rho) + \beta A_{\rho\sigma\gamma}(m_\rho)|^2 d\Pi,$$

$$B(\rho \rightarrow \sigma\gamma) = \frac{m_\rho^2}{\Gamma_\rho^2} \frac{1}{\sigma_\rho} \int |\beta A_{\rho\sigma\gamma}(m_\rho)|^2 d\Pi,$$

$$B(\omega \rightarrow \pi^0\pi^0\gamma) = \frac{m_\omega^2}{\Gamma_\omega^2} \frac{1}{\sigma_\omega} \int |\gamma A_\omega(m_\rho)|^2 d\Pi,$$

where $\sigma_V = 12\pi B(V \rightarrow e^+e^-)/M_V^2$ is a total vector meson production cross section in e^+e^- collisions.

Table 4: The branching ratios of ρ and ω decays ($B \times 10^5$) and $P(\chi^2)$ values obtained as a result of cross section fitting with different values of ϕ_β , ϕ_γ . The $\omega\pi$ amplitude was described by the Model 3 from Table 3. Model 1 from Table 5 was used for description of $\rho \rightarrow \sigma\gamma$ amplitude. Only statistical errors of parameters are shown.

Model		$B(\omega \rightarrow \pi^0\pi^0\gamma)$	$B(\rho \rightarrow \pi^0\pi^0\gamma)$	$B(\rho \rightarrow \sigma\gamma)$	$P(\chi^2)$
1	$\phi_\beta \approx 0, \phi_\gamma \approx 0$	$6.3^{+1.4}_{-1.3}$	$4.1^{+1.0}_{-0.9}$	$1.9^{+0.9}_{-0.8}$	35%
2	$\phi_\beta \approx \pi, \phi_\gamma \approx 0$	$12.3^{+2.3}_{-1.6}$	$3.8^{+0.9}_{-0.8}$	4.4 ± 1.0	30%
3	$\phi_\beta \approx 0, \phi_\gamma \approx \pi$	$25.5^{+2.4}_{-2.3}$	$5.1^{+1.0}_{-0.9}$	1.9 ± 1.0	6%
4	$\phi_\beta \approx \pi, \phi_\gamma \approx \pi$	15.8 ± 2.3	$4.7^{+0.9}_{-0.8}$	$5.6^{+1.1}_{-1.0}$	8%

Characteristic feature of the process under study is a large interference between the contributions of ρ and ω decays. For instance the cross section of $e^+e^- \rightarrow \omega \rightarrow \pi^0\pi^0\gamma$ process at $E = m_\omega$ evaluated using the table value of $B(\omega \rightarrow \pi^0\pi^0\gamma) = (7.2 \pm 2.5) \cdot 10^{-5}$ is equal to 0.12 nb. The interference with ρ meson increases this value up to approximately 0.25 nb (Fig.4). The experimental data on the energy dependence of the cross section are insufficient for determination of unambiguous solution for interference phases ϕ_β , ϕ_γ . There are four solutions listed in Table 4. The third and fourth ones correspond to a large destructive contribution into ω decay from mechanisms other than $\rho^0\pi^0$. The $B(\omega \rightarrow \pi^0\pi^0\gamma)$ values obtained in this case disagree with existing experimental value $B(\omega \rightarrow \pi^0\pi^0\gamma) = (7.2 \pm 2.5) \cdot 10^{-5}$. The solution with $\phi_\beta \approx \pi, \phi_\gamma \approx 0$ can be ruled out for two reasons: $B(\omega \rightarrow \pi^0\pi^0\gamma)$ exceeds the table value by 1.7 standard deviations and consistency of the calculated spectrum of the recoil photon with the experimental one is poor. The analysis of the photon spectrum is described in the next section.

For the only survivor solution with both phases close to zero, the model dependence of the fit parameters was studied. Three models of excited ρ states (Table 3) and four sets of σ parameters (Table 5) were tested. The ϕ_β was found ranging within $(20 \div 80)^\circ \pm 80^\circ$. These values are in agreement with theoretically expected zero value [7]. Therefore the final fitting was performed with $\phi_\beta = 0$. The phase ϕ_γ was considered as a floating parameter to take into account its possible shift due to the contribution of mechanisms other than $\omega \rightarrow \rho\pi^0$. The fitted $\phi_\gamma = -(2 \div 20)^\circ \pm 20^\circ$ is consistent with zero.

The probabilities of the ρ and ω decays into $\pi^0\pi^0\gamma$ obtained with different parameters of σ meson are listed in Table 5. The spreads in parameter values correspond to different models describing $e^+e^- \rightarrow \omega\pi^0$ cross section

Table 5: The probabilities of the ρ and ω decays into $\pi^0\pi^0\gamma$ ($B \times 10^5$) obtained with different parameters of σ meson. The spreads in the parameter values correspond to the models listed in Table 3. Theoretical values of branching ratios are taken from Ref. [7]. The final results with statistical and systematic errors are given in the bottom line of the table.

Model	m_σ MeV	Γ_σ MeV	$B(\omega \rightarrow \pi^0\pi^0\gamma)$	$B(\rho \rightarrow \pi^0\pi^0\gamma)$		$B(\rho \rightarrow \sigma\gamma)$	
				exp.	th.	exp.	th.
L σ M	478	324	6.2-6.5	4.0-4.1	3.8	1.5-1.9	1.5
L σ M	555	540	6.3-6.6	4.2-4.3	2.8	1.9-2.3	0.8
L σ M	478	263	6.2-6.4	4.2-4.3	4.7	1.7-2.1	2.1
χ PT	—	—	6.5-6.9	3.9-4.0	2.9	1.8-2.2	1.0
			$6.6^{+1.4}_{-1.3} \pm 0.6$	$4.1^{+1.0}_{-0.9} \pm 0.3$		$1.9^{+0.9}_{-0.8} \pm 0.4$	

above 1 GeV. All models reproduce the experimental data well. Therefore parameter midrange was taken as a final result. Its spread was regarded as the model error. The branching ratios obtained this way with statistical and systematic errors are listed in the last row of Table 5. The systematic error includes the model error, uncertainties in the detection efficiency and integrated luminosity. The variation of the background level within its systematic error practically does not change the $B(\omega \rightarrow \pi^0\pi^0\gamma)$ central value and results in following additional uncertainties of the ρ meson branching ratios: 7% for $B(\rho \rightarrow \pi^0\pi^0\gamma)$ and 12% for $B(\rho \rightarrow \sigma\gamma)$. Since these uncertainties affect statistical significance of the results they were added to statistical errors. The energy dependence of the cross section in the model with $m_\sigma = 478$ MeV and $\Gamma_\sigma = 324$ MeV is shown in Fig. 4 together with the curve corresponding to $B(\rho \rightarrow \sigma\gamma) = 0$. The $P(\chi^2)$ value for the latter model is equal to 0.5%.

4 The energy and angular spectra

From Table 2 it is seen that selected events are mainly concentrated in two energy regions: 180 events near ω peak and 92 events in the range 920–970 MeV above the $e^+e^- \rightarrow \omega\pi^0$ reaction threshold. The angular and energy distributions in the latter region agree with $\omega\pi^0$ mechanism. Recoil photon spectrum for events from 760–800 MeV energy range is shown in Fig.6. Although this energy region is dominated by ω peak the contributions of both ω and ρ decays must be taken into account to obtain the theoretical spectrum.

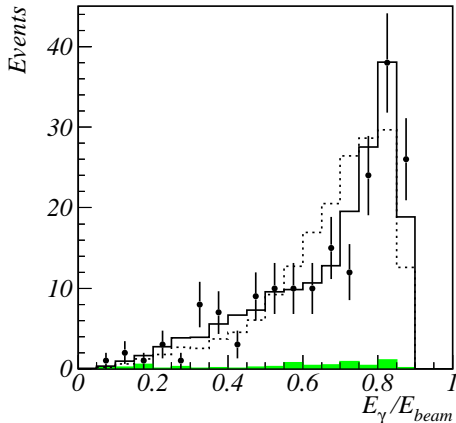


Figure 6: The recoil photon spectrum for the experimental events of the reaction (1) in the energy range $760 < E < 800$ MeV (points with error bars) and the results of simulation in the model 3 from Table 5 (solid line) and in the model 2 from Table 4 (dashed line).

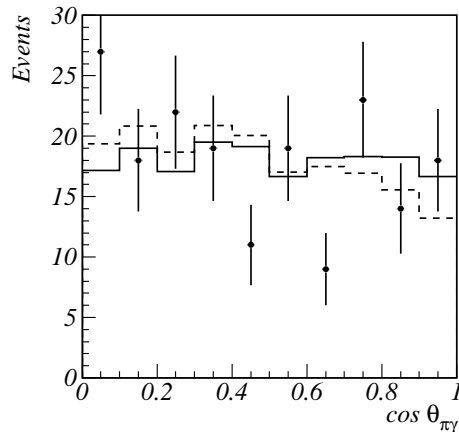


Figure 7: Distribution of cosine angle between photon and π^0 meson in the $\pi^0\pi^0$ rest frame. Point with error bars are experimental data, Solid line is a simulation with ω decay into pure $\rho^0\pi^0$ state. Dashed line is a simulation with ω decaying into a mixture of $\rho^0\pi^0$ and $\sigma\gamma$ states.

The spectrum calculated in model 3 from Table 5 (Fig.6) is in a good agreement with the experimental one. In this model it is supposed that $\omega \rightarrow \pi^0\pi^0\gamma$ decay proceeds through $\rho^0\pi^0$ intermediate state. Another way is to describe the ω decay by a sum of contributions of $\omega \rightarrow \rho^0\pi^0$ and $\omega \rightarrow \sigma\gamma$ mechanisms. To do this we fix $B(\omega \rightarrow \rho^0\pi^0 \rightarrow \pi^0\pi^0\gamma)$ at $2.5 \cdot 10^{-5}$ and fit the $\omega \rightarrow \sigma\gamma$ decay contribution to a value yielding observed $\omega \rightarrow \pi^0\pi^0\gamma$ branching ratio. In case of constructive interference this leads to $B(\omega \rightarrow \sigma\gamma \rightarrow \pi^0\pi^0\gamma) = 1.3 \cdot 10^{-5}$ and the photon spectrum close to that expected for $\rho^0\pi^0$ mechanism. As was shown in the previous section, assumption of destructive interference results in $B(\omega \rightarrow \pi^0\pi^0\gamma)$ inconsistent with the PDG table value.

The second theoretical spectrum in Fig.6 corresponds to the model 2 from Table 4 with destructive interference of $\omega\pi$ and $\sigma\gamma$ amplitudes in ρ decay. For this model the consistency between theoretical and experimental spectra calculated using Kolmogorov test [24] is about 1%, which was one of the reasons to discard this model.

Additional information about mechanism of ω decay can be obtained from the analysis of angular distributions. One of such distribution is shown in Fig.7. The same figure displays the theoretical distributions obtained under assumptions that ω decay proceeds through either pure $\rho^0\pi^0$ intermediate

state or a mixture of $\rho^0\pi^0$ and $\sigma\gamma$. One can see that our limited statistics does not allow to distinguish these two models.

5 Summary

The branching ratios measured in this work,

$$B(\omega \rightarrow \pi^0\pi^0\gamma) = (6.6_{-1.3}^{+1.4} \pm 0.6) \cdot 10^{-5}, \quad (12)$$

$$B(\rho \rightarrow \pi^0\pi^0\gamma) = (4.1_{-0.9}^{+1.0} \pm 0.3) \cdot 10^{-5}. \quad (13)$$

are in a good agreement with our preliminary results [2] and GAMS measurement $B(\rho \rightarrow \pi^0\pi^0\gamma) = (7.2 \pm 2.5) \cdot 10^{-5}$ [3], but have higher accuracy.

The probability of $\rho \rightarrow \pi^0\pi^0\gamma$ decay significantly exceeds VMD model prediction $(1.3 - 1.5) \cdot 10^{-5}$. This excess can be explained by the contribution of the decay via scalar state $\rho \rightarrow \sigma\gamma$. Two mechanisms, $\rho \rightarrow \sigma\gamma$ and $\rho \rightarrow \omega\pi$, can be separated using difference in energy dependence of their amplitudes. Our result on $\rho \rightarrow \sigma\gamma$ decay

$$B(\rho \rightarrow \sigma\gamma \rightarrow \pi^0\pi^0\gamma) = (1.9_{-0.8}^{+0.9} \pm 0.4) \cdot 10^{-5} \quad (14)$$

differs from zero by 2.4 standard deviations and is consistent with the predictions of chiral models [7, 9]. The magnitude of $B(\rho \rightarrow \sigma\gamma)$ is sensitive to σ parameters. As can be seen from Table 5, the models with $\Gamma_\sigma \sim 300$ MeV give the most consistent description of the experimental data.

The value of the branching ratio $B(\omega \rightarrow \pi^0\pi^0\gamma) = (6.7 \pm 1.2) \cdot 10^{-5}$, obtained by averaging of our measurement with the GAMS result exceeds theoretical predictions, $(4.6 \pm 1.1) \cdot 10^{-5}$ [7, 11] and $(4.7 \pm 0.9) \cdot 10^{-5}$ [9], by 1.3 standard deviations. It is necessary to make some remarks about these predictions. The result of Ref. [11] is based on table value of $\Gamma(\rho \rightarrow \pi^0\gamma) = 102 \pm 26$ keV [25]. It must be corrected taking into account newer measurement $\Gamma(\rho \rightarrow \pi^0\gamma) = 76 \pm 22$ keV [26], which is close to the value for charged ρ , $\Gamma(\rho^\pm \rightarrow \pi^\pm\gamma) = 68 \pm 8$ keV [25]. This decreases the predicted $B(\omega \rightarrow \pi^0\pi^0\gamma)$ and worsens agreement with the experiment. In the Refs. [7] and [9] the values of $g_{\rho\omega\pi}$ equal to 15 GeV^{-1} and 15.9 GeV^{-1} were used to calculate $B(\omega \rightarrow \pi^0\pi^0\gamma) \propto g_{\rho\omega\pi}^2 g_{\rho\pi\gamma} \propto g_{\rho\omega\pi}^4 / g_\rho^2$. On the other hand, the use of these $g_{\rho\omega\pi}$ values for VMD calculation of $\Gamma(\omega \rightarrow 3\pi)$ and $\Gamma(\omega \rightarrow \pi^0\gamma)$ leads to too large values conflicting with experimental data. For example, the $g_{\rho\omega\pi}$ obtained from $\omega \rightarrow 3\pi$ width assuming intermediate $\rho\pi$ state is equal to $(14.3 \pm 0.2) \text{ GeV}^{-1}$ [14]. Therefore, our opinion is that $4.6 \cdot 10^{-5}$ is the maximum branching ratio acceptable within VMD model and the additional theoretical study is required to explain the large value of $B(\omega \rightarrow \pi^0\pi^0\gamma)$.

6 Acknowledgments

This work is supported by “Russian Fund for Basic Researches” grants No. 01-02-16934-a and 00-15-96802 and STP “Integration” Fund, grant No. A0100.

References

- [1] M.N. Achasov et al., Nucl. Instr. Meth. A 449 (2000) 125.
- [2] M.N. Achasov et al., JETP Letters, 71 (2000) 355.
- [3] D. Alde et al., Phys. Lett. B 340 (1994) 122.
- [4] P. Singer, Phys. Rev. 128 (1962) 2789.
- [5] A. Bramon, A. Grau, G. Pancheri, Phys. Lett. B 283 (1992) 416.
- [6] A. Bramon, A. Grau, G. Pancheri, Phys. Lett. B 289 (1992) 97.
- [7] A. Bramon et al., Phys. Lett. B 517 (2001) 345.
- [8] E. Marco et al., Phys. Lett. B 470 (1999) 20.
- [9] J. E. Palomar, S. Hirenzaki, E. Oset, e-print hep-ph/0111308.
- [10] A. Gokalp, O. Yilmaz, Phys. Lett. B 508 (2001) 25.
- [11] D. Guetta, P. Singer, Phys. Rev. D 63 (2001) 017502.
- [12] A. Gokalp, O. Yilmaz, Phys. Lett. B 494 (2000) 69.
- [13] A.V. Bozhenok, V.N. Ivanchenko, Z.K. Silagadze, Nucl. Instr. Meth. A 379 (1996) 507.
- [14] M.N. Achasov et al., Nucl. Phys. B 569 (2000) 158.
- [15] E.A. Kuraev, V.S. Fadin, Sov. J. Nucl. Phys. 41 (1985) 466.
- [16] A.B. Clegg, A. Donachie, Z. Phys. C 62 (1992) 455.
- [17] M.N. Achasov et al., Phys. Lett. B 486 (2000) 29.
- [18] K.W. Edwards et al., Phys. Rev. D 61 (2000) 072003.
- [19] Y.S. Tsai, Phys. Rev. D 4 (1971) 2821.

- [20] R. Barate et al., Z. Phys. C 76 (1997) 15.
- [21] S. Anderson et al., Phys. Rev. D 61 (2000) 112002.
- [22] E.M. Aitala et al., Phys. Rev. Lett. 86 (2001) 770.
- [23] D.M. Asner et al., Phys. Rev. D 61 (2000) 012002.
- [24] HBOOK Reference Manual, CERN program library Y250, 1998, p.90.
- [25] Review of Particle Physics. Eur. Phys. J. C 15 (2000) 1.
- [26] M.N. Achasov et al., e-print hep-ex/0109035.